Impact of Distortion on Local Radiomic Analysis of Quadriceps Based on Quantitative Magnetic Resonance Imaging Data

Hoai-Thu Nguyen[1], Sylvain Grange[1,2], Benjamin Leporq[1], Magalie Viallon[1,2], Pierre Croisille[1,2], and Thomas Grenier[1]

[1]Univ Lyon, UJM-Saint Etienne, INSA-Lyon, UCB Lyon 1, CNRS, Inserm, CREATIS UMR 5220, U1206, France
[2]Department of Radiology, Centre Hospitalier Universitaire de Saint-Etienne, UJM-Saint Etienne, Saint-Etienne, France
Email: {hoai-thu.nguyen, thomas.grenier, magalie.viallon, pierre.croisille}@creatis.insa-lyon.fr

***Abstract*—This study investigates the impact of the MRI distortion that appears between 3D T1 Dixon Water-only images and both spoiled gradient echo and multi-echos T2 weighted spin-echo images when sequentially acquired. Recent studies focusing on radiomic features locally computed on muscle heads or bone marrow segmentations require precise corrections of the bias field and the distortion. Our results suggest that classically used rigid registration are not optimal for such fine study and that deformable registration should be preferred to limit significant error in radiomic feature extraction. However, from our experiments on our data, no significant change in radiomic statistic is observed whatever segmentation correction approach was applied. This indicates that radiomic features are not sensitive to segmentation refinement when considering large 3D regions.**

***Index Terms*—radiomics, quantitative maps, registration, magnetic resonance imaging**

I. Introduction

Radiomic features extracted from medical images (MRI, CT, PET, …) enable advanced image-based tissue characterization and objective monitoring in longitudinal studies [1], [2]. Radiomics is a process that involves extracting and analyzing a large quantity of features from medical images [3]. Features extracted from longitudinal quantitative Magnetic Resonance Imaging (qMRI) data can convey information regarding fine evolution of tissues [4] after anatomical segmentations are ideally obtained automatically. While features need to be extracted from many different sequences, the segmentation is generally best being performed on a given contrast. Since the correction of MRI distortion is a well-known challenge in Magnetic Resonance (MR) image analysis [5], [6], which make feature extraction by superposing automatic segmentation obtained on one sequence on the other sequences questionable, our objective is to investigate the impact of such distortion in our study hence to find the most suitable registration framework [7], [8] minimizing contamination from misclassified structure due to potential distortion in order to obtain the purest radiomic data best describing each compartment of interest.

Our study involves the upper leg MR images of ultra-marathoners and focuses on the quadriceps muscles segmentation which is a laborious task when performed either manually or automatically. This paper is organized as follow: In the next section, we will describe our data and preprocessing. Then the registration scheme will be detailed. The Section IV will describe the extracted radiomic features. Finally, we disclose and discuss our results.

II. Data

Our data was collected from 50 runners of the Mountain ultra-marathon (MUM) Tor Des Géants 2014 (330km, 24.000 m of elevation gain) who volunteered to participate in the study which consisted of image acquisition and biological analysis at multiple time points during and after the race. Among the 50 runners, only 30 finished the race and after data quality control, we conserved 20 finishers for our study.

Therefore, our MRI data included 3D T1 Dixon Water only (2-points Dixon, 160 coronal slices) MR images collected from these 20 finishers then corrected using N4 bias field correction [9], as well as quantitative maps [10] of T2* derived from 3D spoiled gradient echo sequences (3DGre) and of T2 derived from 2D multi-echos T2 weighted spin-echo sequences. It is important note that based on the physical properties of MR acquisition, the morphological structures perfectly represented in T1 Dixon sequences are deformed intrinsically in multi-echos T2 spin-echo ones. In addition, the different sequences have different resolutions and different field of views. A semi-automatic segmentation of the four quadriceps muscle heads was performed on the T1 Dixon Water-only (T1w) images [11] on both legs. Example of quadriceps muscles segmentation can be found in Fig. 1. Below, we will analyze radiomic change on 8 muscle heads (4 on each leg) plus one (denoted as “All”, which represents all quadriceps muscle heads together) corresponding to the grouping of all muscles when the

Manuscript received November 27, 2020; revised Feburary 3, 2021.

doi: 10.18178/ijpmbs.10.2.49-54

segmentations are coarsely then finely registered on quantitative maps.

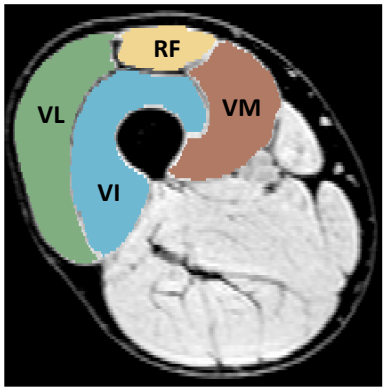

Figure 1. T1w and segmentations of the 4 quadriceps muscle heads: VL - Vastus Lateralis, RF - Rectus Femoris, VM - Vastus Medialis, VI - Vastus Intermedius.

III. Image Registration

Our registration pipeline is described in Fig. 2 where no intensity change is performed on data from which radiomic features will be extracted. Here we study rigid then deformable B-spline registrations from T1w images to T2* and T2 maps. During registration process, the mutual information was maximized using an adaptive stochastic gradient ascent with a 4-scales multi-resolution scheme. The use of mutual information is mandatory due to the important permutation of intensity range between T1w and the quantitative maps [8]. The mutual information can be defined with the following formula:

$$MI(A,B) = H(A) + H(B) - H(A,B)$$

where $H(A)$ and $H(B)$ are margina entropies of images A and B respectively and $H(A,B)$ is their joint entropy. The entropies are defined as:

$$H(A) = -\int p_A(a)\log p_A(a)da$$

$$H(B) = -\int p_B(b)\log p_B(b)db$$

$$H(A,B) = -\int p_{AB}(a,b)\log p_{AB}(a,b)dadb$$

where p_A , p_B and p_{AB} are respectively marginal probability density functions for A and for B and their joint probability density function. Here, these functions were constructed using the method of Mattes et al. [12]: probability density distribution were estimated using Parzen windowing. The larger the MI, the better aligned the two images.

The 4-scales multi-resolution scheme ensures a robust convergence of gradient ascent on our data for both rigid and deformable transformation. The rigid registration allows translation and rotation while the deformable registration allows local changes modeled by a Free-Form Deformation (FFD) based on B-spline functions. Let the image volume be denoted as $\Omega = \{(x,y,z) \mid 0 \le x < X, 0 \le y < Y, 0 \le z < Z\}$. The basic idea of FFD is to manipulate a mesh ϕ of $n_x \times n_y \times n_z$ control points $\phi_{i,j,k}$ of Ω. The FFD can be written as the 3D-tensor product of the familiar 1-D cubic B-splines [13]:

$$T_{local}(x,y,z) = \sum_{l=0}^{3}\sum_{m=0}^{3}\sum_{n=0}^{3} B_l(u)B_m(u)B_n(u)\phi_{i+l,j+m,k+n}$$

where $i = \lfloor x/n_x \rfloor$, j= $\lfloor y/n_y \rfloor$, $k = \lfloor z/n_z \rfloor$, $u = x/n_x - \lfloor x/n_x \rfloor$, $v = y/n_y - \lfloor y/n_y \rfloor$, $w = z/n_z - \lfloor z/n_z \rfloor$ and B_l represents the lth basis function of B-spline:

$$B_0(u) = (1-u)^3/6$$

$$B_1(u) = (3u^3 - 6u^2 + 4)/6$$

$$B_2(u) = (-3u^3 + 3u^2 + 3u + 1)/6$$

$$B_3(u) = u^3/6$$

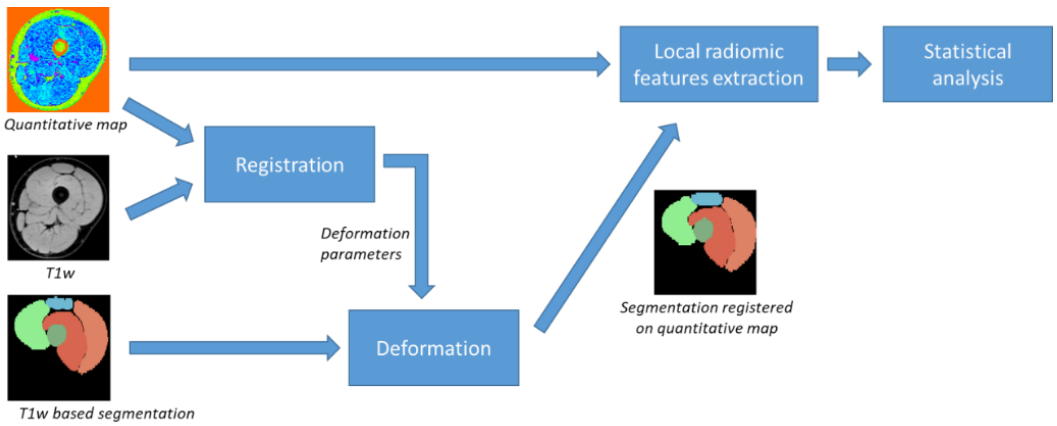

Figure 2. Proposed registration pipeline to study the effect of registration method on radiomic features. Note that the N4 bias field correction of the T1w was performed beforehand.

In our application, one control point was set every 25 voxels so $n_x = \lceil X/25 \rceil$, $n_x = \lceil Y/25 \rceil$ and $n_z = \lceil Z/25 \rceil$. This subsampling allows obtaining not too small and unrealistic deformations in accordance with the muscles' shape and MRI distortion.

After the registration process, the obtained deformation fields were applied to the semi-automatic segmentations using a k-nearest neighbor interpolator to preserve integer values.

One can note that deforming the segmentation only does not affect intensity values of the MRI quantitative maps from which radiomic features will be extracted.

IV. Radiomic Features Extraction

Radiomic features were extracted from each segmented quantitative maps T2 and T2*, including distribution and texture features. Features were computed on the total 3D volumes using the toolbox and recommendations of Vallières *et al.* [3]. Each slice were quantitated on 32 gray levels using Lloyd-Max quantization algorithm [14], [15] to define decision thresholds in the volume. Next, four matrices were built:

- GLCM (Gray-level co-occurrence matrix): represents the number of times the combination of 2 different gray levels occurs in two voxels next to each other,
- GLRLM (Gray-level run length matrix): quantifies the length, in number of consecutive voxels, of a gray level in the considered volume
- GLSZM (Gray-level size zone matrix): quantifies gray level zones in an image. Unlike GLCM and GLRLM, this matrix is rotation invariant,
- NGTDM (Neighborhood gray-tone difference matrix): analyzes the difference between the gray level of a voxel and the average gray level of its neighbors.

The four matrices were constructed using the 26-voxel connectivity and in 13 directions of 3D space (the 13 are accumulated on each matrix). Overall, from each MRI quantitative map, 55 distributions and texture features were extracted for each of 9 volumes (8 muscle heads plus one for the entire muscle volume) as: mean, variance, entropy, energy, correlation, etc. (reader can refer to [9] for the complete listing).

It is important to note that most of such features are moment of the matrices elements leading to average. As the matrices are computed in 3D on each whole muscle head volume, changes at the boundaries of the segmentation will involve few pixels and thus we can expect that small to no change would be observed on radiomic features.

Finally, the 55 radiomic features were extracted using unregistered and registered segmentations on each muscle head. We then compared radiomic values obtained with both registration schemes using the Wilcoxon signed-rank test since normal distribution condition is not met here and since we have only 20 subjects in our study. The segmentations themselves were also compared with each other using DICE scores in order to assess their similarity (a DICE score of 1.0 means that the two compared segmentations are identical). Finally, mutual information values between T1w and quantitative maps before and after registrations were used to assess the alignment quality of MRIs.

V. Implementation

The registration, DICE and mutual information calculations, feature extraction and comparison were programmed using elastix [16], C++/ITK [17], MATLAB [3] and R [18] respectively.

VI. Results and Discussion

Visual assessment of distortion before and after registration can be examined on Fig. 3. These observations should be made discretely as T2 and T2* are noisy and do not highlight the same information as T1w. Without registration, it has to be kept in mind that T2* map is less affected by distortion artefact than the one of T2. In average, both registration approaches improved the matching with the T1w image, as confirmed by the improvement of the Mutual Information (MI) values of Table I.

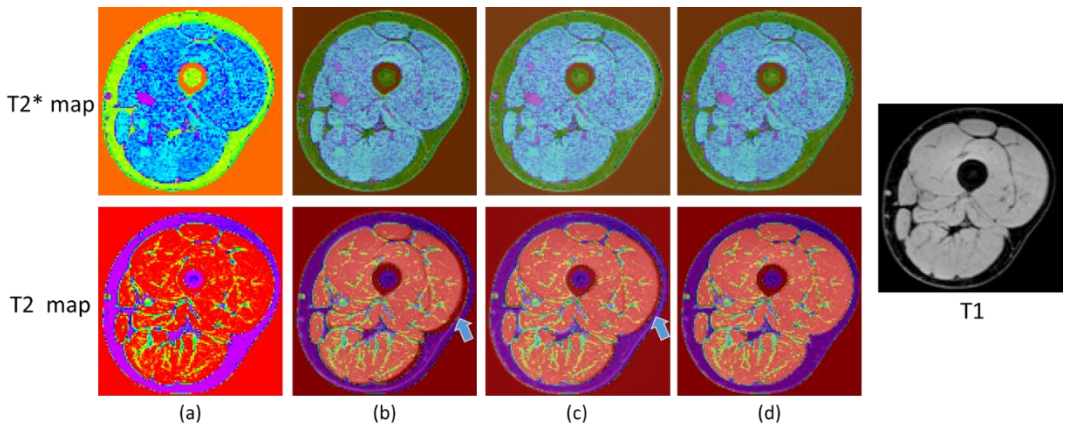

Figure 3. T2 and T2* maps (a) and T1w image (on the right) of the left leg of a runner. By superposing T1w image on the quantitative maps, we can observe the original distortions between T1w and T2 maps (b), distortions after rigid registration (c) and after deformable registration (d). The arrows guides to the visually observable distortions. The distortions between T1w and T2* map are not as visible. T2 and T2* maps are displayed in colors for better visualization.

Only for 3 runners rigid transform failed to improved MI using T2 and for 8 runners (40%) considering T2* maps (bold values in Table I). We note that deformable registration based on B-spline always provided highest mutual information value, implicating that it was robust and it improved image alignment (except for MAV, where registration did not converge as expected but still produced a visually satisfying registration, as show in Fig. 4). The changes in segmentation overlap with and without registration were also non-negligible considering the DICE scores in the Table II.

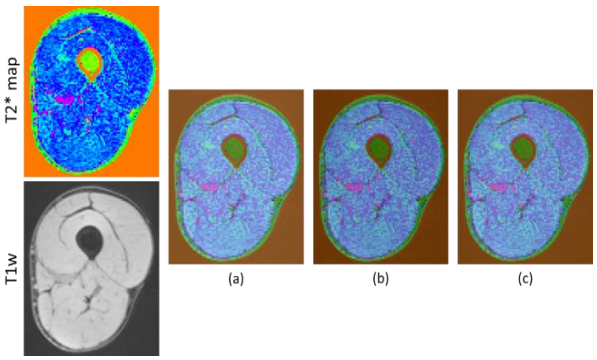

Figure 4. An axial slice T2* maps and T1w image (on the right) of the left leg of the runner MAV, and the resulted visualization by superposing T1w on T2* before registration (a), after a rigid registration (b) and after a deformable registration (c).

TABLE I. MUTUAL INFORMATION VALUES BETWEEN T1W AND UNREGISTERED/REGISTERED (RIGID OR B-SPLINE) QUANTITATIVE MAPS (T2 AND T2*) FOR ALL STUDIED RUNNERS. BOLD VALUES ARE SPECIAL CASE WHERE REGISTRATION DID NOT IMPROVE IMAGE SIMILARITY

Name	T2 none	T2 rigid	T2 BSpline	T2* none	T2* Rigid	T2* BSpline
ALB	0,720	0,739	0,774	0,766	**0,746**	0,775
ALF	0,647	**0,565**	0,661	0,713	**0,701**	0,720
ARS	0,795	0,832	0,875	0,756	0,770	0,814
BRG	0,729	0,770	0,782	0,772	0,779	0,804
CHS	0,647	**0,619**	0,731	0,708	0,733	0,789
CLB	0,713	**0,709**	0,729	0,783	**0,754**	0,803
EMS	0,665	0,730	0,774	0,750	0,777	0,821
ERT	0,752	0,830	0,849	0,798	0,809	0,834
FAP	0,711	0,751	0,772	0,776	0,787	0,820
MAC	0,621	0,710	0,740	0,704	**0,703**	0,727
MAJ	0,705	0,794	0,827	0,781	0,798	0,831
MAP	0,609	0,626	0,656	0,777	**0,756**	**0,777**
MAV	0,589	0,652	0,711	0,743	**0,679**	**0,694**
OUK	0,725	0,789	0,806	0,793	**0,793**	0,816
PAC	0,679	0,722	0,733	0,753	0,758	0,781
PIS	0,736	0,791	0,851	0,773	0,790	0,827
ROE	0,711	0,805	0,830	0,808	0,833	0,864
THB	0,732	0,827	0,853	0,808	0,835	0,873
VAH	0,598	0,681	0,743	0,704	0,730	0,781
YAG	0,756	0,820	0,837	0,780	**0,779**	0,810
Mean	0,692	0,738	0,777	0,762	0,766	0,798
stdev	0,058	0,078	0,064	0,033	0,042	0,045

TABLE II. DICE SCORES COMPUTED AGAINST UNREGISTERED AND REGISTERED SEGMENTATIONS FOR ALL STUDIED RUNNERS

Name	T2 none	T2 rigid	T2 BSpline	T2* Rigid	T2* BSpline
ALB	1	0,931	0,932	0,969	0,953
ALF	1	0,837	0,904	0,978	0,969
ARS	1	0,959	0,946	0,977	0,957
BRG	1	0,958	0,957	0,980	0,970
CHS	1	0,781	0,832	0,938	0,930
CLB	1	0,960	0,956	0,986	0,970
EMS	1	0,936	0,933	0,956	0,947
ERT	1	0,947	0,944	0,974	0,962
FAP	1	0,943	0,941	0,968	0,963
MAC	1	0,893	0,886	0,961	0,949
MAJ	1	0,946	0,942	0,975	0,962
MAP	1	0,929	0,916	0,964	0,958
MAV	1	0,799	0,805	0,981	0,974
OUK	1	0,949	0,945	0,977	0,969
PAC	1	0,950	0,948	0,974	0,961
PIS	1	0,924	0,914	0,975	0,960
ROE	1	0,933	0,936	0,974	0,963
THB	1	0,952	0,948	0,964	0,957
VAH	1	0,892	0,889	0,942	0,933
YAG	1	0,953	0,952	0,973	0,961
Mean	1	**0,919**	**0,921**	**0,969**	**0,958**
stdev	0	0,0529	0,0410	0,0123	0,0116

Despite such changes in segmentations, most of the radiomic features computed on T2 and T2* maps using the registered and unregistered segmentations revealed almost no statistically significant change (Fig. 5) with some significant results for the left VL (6/55 for T2* and 3/55 for T2). Considering the noisiness of the quantitative maps, especially at the border that separate muscles and fat/skin, and the fact that most of the features with significant changes (min, variance, intensity range) are sensitive to noise, we can consider overlooking these results and can conclude that reducing the distortion between T1w and T2 and T2* do not have any impact on the radiomics and the segmentation quality (in absence of major segmentation errors) does not influent the radiomic features in the quadriceps.

Nevertheless, the entire muscle volume in T2* maps contains, in average, 200.000 voxels and this number is at 80.000 in T2 maps. Meanwhile, the MRI distortion usually involves a small part at the boundary of muscle volume. Also, the 55 radiomic features were computed in a 3D manner using the whole set of pixels of each muscle head volume and were averaged when necessary. From our observation, such features are not suitable to highlight small variations when volume's boundaries evolve as it can be intuitively explained while looking at the definition of radiomic feature calculation: noise, resolution, binning and averaging do not allow describing tissues variation at region boundaries or small changes in tissues.

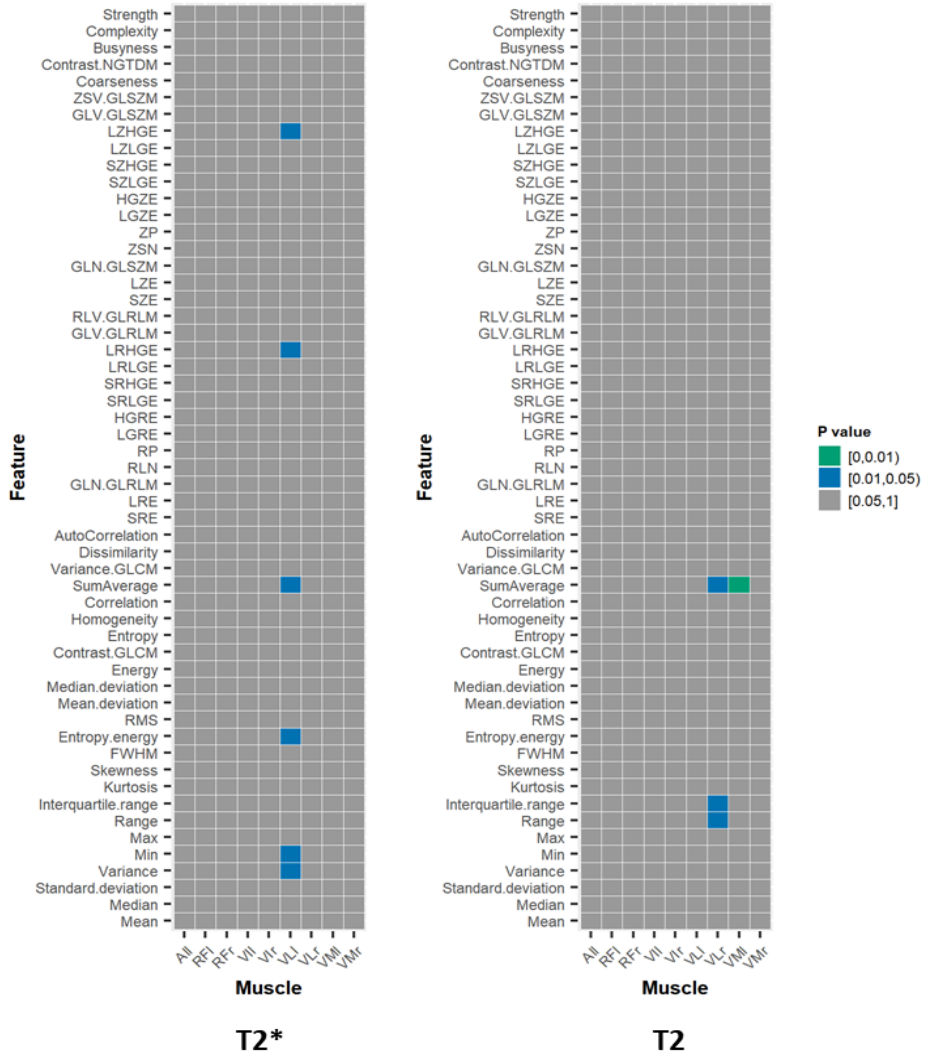

Figure 5. P values of statistical tests comparing the radiomic features extracted from each muscle volumes on T2* and T2 map using segmentations of T1w before and after a deformable registration. A P value inferior to .05 indicates significant difference. Abbreviations: VL - Vastus Lateralis, RF - Rectus Femoris, VM - Vastus Medialis, VI - Vastus Intermedius, r – right, l – left legs.

VII. Conc lusion

We studied the impact of two different intra registration approaches to reduce the MRI distortion between T1w and T2 and T2* quantitative maps for extraction of local individual quadriceps radiomic features from quantitative maps.

On the 20 studied cases, our results suggest that considering robustness and segmentation mask alignment tasks, registration must be performed in a deformable way. However, when focusing on radiomic features computed on each quadriceps volumes in a 3D manner, the correction of the distortion does not yield in any statistically significant modifications.

Conflict of Interest

The authors declare no conflict of interest.

Author Contributions

Magalie Viallon and Pierre Croisille acquired the data; Benjamin Leporq and Magalie Viallon computed the quantitative maps; Hoai-Thu Nguyen and Sylvain Grange conducted the research; Hoai-Thu Nguyen programmed the pipeline; Hoai-Thu Nguyen and Thomas Grenier analyzed the data and wrote the paper; all authors had contributed to and approved the final version.

References

[1] J. E.V. Timmeren, *et al.*, "Longitudinal radiomics of cone-beam CT images from non-small cell lung cancer patients: Evaluation of the added prognostic value for overall survival and locoregional recurrence," *Radiother. Oncol.*, vol. 136, pp. 78-85, 2019.

[2] S. H. Bak, H. Park, I. Sohn, S. H. Lee, M. J. Ahn, and H. Y. Lee, "Prognostic impact of longitudinal monitoring of radiomic features in patients with advanced non-small cell lung cancer," *Sci. Rep.*, vol. 9, p. 8730, 2019.

[3] M. Vallières, C. R. Freeman, S. R. Skamene, and I. E. Naqa, "A radiomics model from joint FDG-PET and MRI texture features for the prediction of lung metastases in soft-tissue sarcomas of the extremities," *Phys. Med. Biol.*, vol. 60, no. 14, pp. 5471-5496, 2015.

[4] H. T. Nguyen, *et al.*, "Longitudinal study of quadriceps muscle head inflammation of athletes enrolled in extreme mountain ultra-marathon using radiomic features extracted from automatic segmentation based on atlas registration and machine learning of

MR Images," in *ELMSK : Exercise, Locomotion and Musculoskeletal System*, 2018.
[5] A. Walker, G. Liney, P. Metcalfe, and L. Holloway, "MRI distortion: Considerations for MRI based radiotherapy treatment planning," *Australas. Phys. Eng. Sci. Med.*, vol. 37, pp. 103-113, 2014.
[6] S. Rizzo, *et al.*, "Radiomics: The facts and the challenges of image analysis," *European Radiology Experimental*., vol. 2, p. 36, 2018.
[7] E. Dohmatob, G. Varoquaux, and B. Thirion, "Inter-subject registration of functional images: Do we need anatomical images?" *Front. Neurosci.*, vol. 12, p. 64, 2018.
[8] J. P. W. Pluim, J. B. A. A. Maintz, and M. A. Viergever, "Mutual-information-based registration of medical images: A survey," *IEEE Transactions on Medical Imaging*, vol. 22, no. 8, pp. 986-1004, 2003.
[9] N. J. Tustison, *et al.*, "N4ITK: Improved N3 bias correction," *IEEE Trans. Med. Imaging*, vol. 29, no. 6, pp. 1310-1320, 2010.
[10] B. Leporq, *et al.*, "Combined quantification of fatty infiltration, T 1-relaxation times and T 2*-relaxation times in normal-appearing skeletal muscle of controls and dystrophic patients," *Magn. Reson. Mater. Physics, Biol. Med.*, vol. 30, no. 4, pp. 407-415, 2017.
[11] B. Gilles, C. D. Bourguignon, P. Croisille, G. Millet, O. Beuf, and M. Viallon, "Automatic segmentation for volume quantification of quadriceps muscle head: A longitudinal study in athletes enrolled in extreme mountain ultra-marathon," in *ISMRM: International Society for Magnetic Resonance in Medicine*, 2016.
[12] D. Mattes, D. R. Haynor, H. Vesselle, T. K. Lewellyn, and W. Eubank, "Nonrigid multimodality image registration," in *Proc. SPIE Med. Imaging*, San Diego, 2001.
[13] D. Rueckert, L. I. Sonoda, C. Hayes, D. L. Hill, M. O. Leach, and D. J. Hawkes, "Nonrigid registration using free-form deformations: Application to breast MR images," *IEEE Trans. Med. Imaging*, vol. 18, no. 8, pp. 712-721, 1999.
[14] S. P. Lloyd, "Least squares quantization in PCM," *IEEE Trans. Inf. Theory*, vol. 28, no. 2, pp. 129-137, 1982.
[15] J. Max, "Quantizing for minimum distortion," *IRE Trans. Inf. Theory*, vol. 6, no. 1, pp. 7-12, 1960.
[16] S. Klein, M. Staring, K. Murphy, M. A. Viergever, and J. P. W. Pluim, "Elastix: A toolbox for intensity-based medical image registration," *IEEE Trans. Med. Imaging*, vol. 29, no. 1, pp. 196-205, 2010.
[17] T. S. Yoo, *et al.*, "Engineering and algorithm design for an image processing API: A technical report on ITK - The insight toolkit," *Studies in Health Technology and Informatics*, vol. 85, pp. 586-592, 2002.
[18] The R Core Team, *R: A Language and Environment for Statistical Computing*, Vienna, Austria, 2019.

Hoai-Thu Nguyen received her Engineering degree in Bioinformatics and Modelization in 2015 from INSA de Lyon (National Institute for Applied Sciences of Lyon), France, her M.Sc. in In vivo Imaging in 2016 from Sorbonne University, Paris, France and her M.Sc. in Data Mining in 2017 from Lumière University Lyon 2, France. Currently she is persuing a Ph.D degree in Medical Imaging at Jean Monnet University of Saint Etienne and CREATIS Laboratory. Her main ares of research include image segmentation, machine learning and data analysis.

Dr. Sylvain Grange obtained his medical doctorate in diagnostic and interventional radiology, with a specialization in muscular and osteoarticular imaging. His research interests focused on muscle imaging, particularly the Magnetic Resonance Imaging and the muscle injuries. Since 2017, he is Ph.D student between the CREATIS Laboratory (UMR CNRS 5220 – INSERM U1206, F-69621, Villeurbanne, France) and the Inter‐university Laboratory of Human Movement Science (LIBM EA 74), University of Lyon, University Jean Monnet, F-42023. Saint Etienne, France.

Dr. Benjamin Leporq has received his PhD degree in 2012 at the University of Lyon (France). His thesis, achieved at CREATIS laboratory, dealt with the development of MRI methods for the diagnosis and the monitoring of chronic liver diseases. He introduced and patented the quantification of the triglyceride fatty acid composition in MRI and developed the quantification of magnetic susceptibility for body applications. For the development of a virtual liver biopsy in non-alcoholic fatty liver diseases, he then pioneered a method to quantify them simultaneously and named this concept "integrated multiparametric MRI". He also initiated and patented the simultaneous quantification of hepatic perfusion and whole transport function with dynamic gadoxetate enhanced MRI. From 2018, he is a research scientist at French national institute of health and medicine research (Inserm) and will work about the extension of the integrated multiparametric imaging concept to other parameters for the mapping of tumor biology and about its association with radiomics and artificial intelligence for precision medicine.

Prof. Dr. Pierre Croisille has been involved in various European and international projects in cardiac MR imaging. He has now more than 20 years of experience in the field of cardiac MRI, and he is currently coordinating different advanced projects on heart diffusion like the "Must project" and is actively promoting the transfer of basic knowledge toward clinical needs. He is author and co-author of over 200 publications focused on methodological, clinical and experimental applications of cardiac imaging. His position titles include Professor of Radiology, Chairman of Nuclear Medicine and Radiology, Chief of Radiology, University Hospital Saint-Etienne. Deputy Directory, CREATIS Research Lab, CNRS 5220 INSERM 1206 Université de Lyon, Université Jean Monnet, INSA Lyon. Pierre is leading the IDM4 transversal project at CREATIS.

Dr. Magalie Viallon worked for 6 years at Siemens HealthCare as clinical scientist. She brought to the "MUST project" a long experience in the field of functional MRI. She was responsible for the methodological development and imaging technologies that were implemented for the project. She is co-author of more than 80 articles targeting different applications of MRI. From 2006 to 2014, she was responsible for the technical, methodological and scientific coordination of the MRI platform of the Radiology Department of the University Hospital of Geneva. She is currently working as an MR physicist in the University Hospital of Saint-Etienne, and as a researcher in the research laboratory CREATIS, UMR5220 INSERM1206.

Dr. Thomas Grenier received his Engineering degree in Electrical Engineering from ISTASE (now Telecom Saint-Etienne) in 2001, his M.Sc. in Image Processing from the University of Saint-Etienne in 2001 and his Ph.D degree in Image Processing from the National Institute for Applied Sciences of Lyon (INSA-Lyon, France) in 2005. He has been working at CREATIS Laboratory since 2001. His research interests are in the field of image segmentation, clustering and filtering, particularly in methods involving feature space and scale space approaches and deep learning approaches. Currently he is associate professor in Electrical Engineering Department at INSA de Lyon. He is the head of the last year major in Signal and Image Processing of the department.